Refinement of Borate Structures from ^{11}B MAS NMR Spectroscopy and Density Functional Theory Calculations of ^{11}B Electric Field Gradients

Michael Ryan Hansen,[†] Georg K. H. Madsen,[‡] Hans J. Jakobsen,[†] and Jørgen Skibsted[†,*]

Instrument Centre for Solid-State NMR Spectroscopy, Department of Chemistry, University of Aarhus, DK-8000 Aarhus C, Denmark, and Department of Inorganic Chemistry, Department of Chemistry, University of Aarhus, DK-8000 Aarhus C, Denmark

Received: September 17, 2004; In Final Form: December 10, 2004

The refinement of borate structures using DFT calculations combined with experimental ^{11}B quadrupole coupling parameters from solid-state NMR spectroscopy is presented. The ^{11}B electric field gradient (EFG) tensors, calculated using the WIEN2k software for trigonal and tetrahedral boron sites in a series of model compounds, exhibit a convincing linear correlation with the quadrupole coupling tensor elements, determined from ^{11}B MAS NMR spectra of the central or satellite transitions. The model compounds include $Li_2B_4O_7$, $Mg_2B_2O_5$, $Mg_3B_2O_6$, $NH_4B(C_6H_5)_4$, and colemanite ($CaB_3O_4(OH)_3{\cdot}H_2O$). The ^{11}B quadrupole moment, $Q = 0.0409 \pm 0.0002$ barn, derived from the linear correlation, is in excellent agreement with the accepted value for $Q(^{11}B)$. This demonstrates that DFT (WIEN2k) calculations can provide precise ^{11}B quadrupole coupling parameters on an absolute scale. On the other hand, DFT calculations based on the reported crystal structures for datolite ($CaBSiO_4(OH)$) and danburite ($CaB_2Si_2O_8$) cannot reproduce the experimental ^{11}B quadrupole coupling parameters to the same high precision. However, optimization of these structures by minimization of the forces between the atoms (obtained by DFT) results in a significant improvement between the calculated and experimental ^{11}B quadrupole coupling parameters, which indicates that reliable refinements of the borate structures are obtained by this method. Finally, the DFT calculations also provide important structural information about the sign and orientation of the EFG tensor elements in the crystal frame, a kind of information that cannot be achieved from ^{11}B NMR experiments on powdered samples.

1. Introduction

Borates are industrially important materials mainly used in the production of a variety of glasses such as heat resistant glasses, ceramic glasses, and optical glasses. Other applications include borates used in herbicides, insecticides, fertilizers, detergents, and laser materials.[1] Furthermore, an increasing number of new materials are reported where borate units are incorporated into zeolites,[2,3] open framework aluminophosphates ($AlPO_4$'s),[4,5] and catalytic support materials (e.g., alumina)[5−7] to modify the acidic properties and thereby the catalytic activities for these materials. Borates contain trigonal BO_3 and/or tetrahedral BO_4 units, which can form a wide number of different structures ranging from isolated orthoanions to chains, rings, layers, and frameworks of these units. These structural types of BO_3 and BO_4 groups are found in crystalline alkali-metal borates, borate minerals as well as borate glasses.

Solid-state ^{11}B NMR spectroscopy has become a key technique in the characterization of borate glasses as a result of the lack of long-range order in these materials. Early studies have shown that BO_3 and BO_4 units can be distinguished by their ^{11}B quadrupole coupling parameters,[8−10] which reflect the interaction between the nuclear electric quadrupole moment (Q) and the electric field gradient (EFG) tensor (**V**) at the nuclear site. The quadrupole coupling tensor is a traceless second-rank tensor that can be expressed by the quadrupole coupling constant, $C_Q = eQV_{zz}/h$, and the asymmetry parameter, $\eta_Q = (V_{yy} - V_{xx})/V_{zz}$, which describe the magnitude and symmetry of the interaction, respectively, and thereby the distortion of the local BO_3 and BO_4 units. Generally, BO_4 tetrahedra in borates exhibit $C_Q(^{11}B)$ values less than 1 MHz whereas BO_3 groups possess quadrupole couplings in the range $2.4 \lesssim C_Q \lesssim 3.0$ MHz.[10−17] Furthermore, the two types of boron environments can be distinguished by the ^{11}B isotropic chemical shifts (δ_{iso}) because BO_3 units resonate in the range $12 \lesssim \delta_{iso} \lesssim 25$ ppm, whereas BO_4 groups exhibit shifts in the approximate range $-4 \lesssim \delta_{iso} \lesssim 6$ ppm. This implies that separate resonances for BO_3 and BO_4 species generally can be achieved by high-speed ^{11}B MAS NMR at high/intermediate magnetic fields ($B \gtrsim 9.4$ T),[12,18] which facilitates the quantification of these species in borate materials.

Attempts to relate the C_Q, η_Q, and δ_{iso} ^{11}B parameters to effects from the second coordination sphere of boron have been less successful. In a recent investigation of BO_3 units in a series of anhydrous binary borates, Kroeker and Stebbins[16] observed that δ_{iso} tends to decrease with increasing condensation of the BO_3 units, i.e., with the replacement of nonbridging oxygens with bridging oxygen atoms in the structures. However, similar interpretations of the quadrupole coupling parameters in terms of structural parameters, characterizing the second coordination sphere for boron, have so far not been proposed.

In this work we report a new approach for interpretation of ^{11}B quadrupole coupling data where these parameters are used as the basis for a refinement of borate structures, employing calculations of the electron density using density functional theory (DFT). The computational approach is based on the

* Correspondence author. Fax: +45 8619 6199. Tel: +45 8942 3900. E-mail: jskib@chem.au.dk.
† Instrument Centre for Solid-State NMR Spectroscopy.
‡ Department of Inorganic Chemistry.

10.1021/jp045767i CCC: $30.25
Published on Web 02/11/2005

linearized augmented plane wave (LAPW) method, as implemented in the WIEN2k code.[19] The C_Q and η_Q ^{11}B parameters are determined with high precision from ^{11}B MAS NMR spectra of the central transition (BO_3 units) or the satellite transitions (BO_4 units), providing the principal elements of the quadrupole coupling tensors. When the crystal structures have been reported with good accuracy, it is shown that these elements give a 1:1 correlation with the calculated principal elements for a number of borates. This observation forms the basis for a DFT refinement of less accurate crystal structures by minimization of the forces between nuclei. The approach employs the atomic positions from earlier reported XRD structures as input and we show that an excellent agreement is obtained between the experimental and calculated ^{11}B quadrupole tensor elements for the refined structures. This is demonstrated for the borate minerals datolite ($CaBSiO_4(OH)$) and danburite ($CaB_2Si_2O_8$). It is expected that this approach will find widespread applications in studies of other spin quadrupolar nuclei such as ^{17}O, ^{23}Na, ^{27}Al, and ^{51}V for a range of inorganic materials.

Within the past few years, the WIEN2k package has been increasingly employed for calculation of a variety of physical and spectroscopic properties derived from the electron densities for a range of inorganic crystalline materials including metals, alloys, semiconductors, and minerals.[20] This package, based on the LAPW approach, has already proven high precision in calculations of EFG tensors.[21−23] In a recent study of the five- and six-coordinated Al sites in andalusite (Al_2SiO_5), using ^{27}Al single-crystal NMR and DFT (WIEN97) calculations, a very good agreement between the experimental and calculated EFG tensor orientations has been reported for both Al sites.[24] In the present work we demonstrate that an excellent agreement between experimental and calculated ^{11}B parameters can be obtained for a series of model compounds. This validates the method and provides a detailed understanding of the relation between structure and EFG tensor elements. Furthermore, as a result of the high sensitivity of the EFG tensor to the structural environment of the quadrupole nucleus, it is an intriguing approach to validate theoretically optimized structures by comparing their calculated EFGs with experimentally determined quadrupole coupling parameters of high precision. This is demonstrated in this work by optimization of the structures for $Li_2B_4O_7$, datolite, and danburite.

2. Experimental Section

Materials. $Li_2B_4O_7$ was purchased from Aldrich (Milwaukee, WI) and used without further purification. $Mg_2B_2O_5$ and $Mg_3B_2O_6$ were prepared from stoichiometric mixtures of $Mg(OH)_2$ and H_3BO_3. The triclinic form of $Mg_2B_2O_5$ was obtained by slowly heating the reagents to 1200 °C and keeping the mixture at this temperature for 5 h. The temperature was subsequently lowered to 1000 °C and the mixture was annealed at this temperature following the procedure reported by Guo et al.[25] For $Mg_3B_2O_6$ the reagents were heated to 1200 °C, kept at this temperature for 12 h, and slowly cooled to room temperature. The sample was ground and the heating scheme repeated once. The sample of danburite (Chareas, Mexico) was kindly provided by the Geological Museum, University of Copenhagen, Denmark. The structures and basic purities of the samples were confirmed by powder X-ray diffraction.

NMR Spectroscopy. Solid-state ^{11}B MAS NMR spectra were obtained on Varian *Unity* INOVA-300 (7.1 T) and -600 spectrometers (14.1 T) using home-built CP/MAS probes for 5 mm and 4 mm o.d. rotors, respectively. The spectra employed short rf pulse widths of $\tau_p = 0.5-1.0$ μs for a rf field strength of $\gamma B_1/2\pi \approx 65$ kHz and ^{1}H decoupling ($\gamma B_2/2\pi \approx 50$ kHz). The magic angle was adjusted by minimizing the line widths for the spinning sidebands in the ^{23}Na MAS NMR spectrum of $NaNO_3$ while stable spinning frequencies were achieved using the Varian rotor-speed controller. The ^{11}B isotropic chemical shifts are in ppm relative to neat $F_3B{\cdot}O(CH_2CH_3)_2$ employing a 0.1 M H_3BO_3 aqueous solution ($\delta_{iso} = 19.6$ ppm)[16,26] as a secondary, external reference sample. The numerical analysis (simulations, least-squares optimizations, and error analysis) of the ^{11}B MAS NMR spectra were performed using the *STARS* software.[27−29] The quadrupole coupling parameters are defined as

$$C_Q = \frac{eQV_{zz}}{h} \qquad \eta_Q = \frac{V_{yy} - V_{xx}}{V_{zz}} \tag{1}$$

where Q is the nuclear quadrupole moment and $|V_{zz}| \geq |V_{xx}| \geq |V_{yy}|$. The elements of the EFG tensor (V_{ij}) are the second derivatives with respect to the electric potential ($V(x,y,z)$) produced by the electrons at the nuclear site, i.e., $V_{ij} = \partial^2 V(x,y,z)/\partial x_i \partial x_j$, $i, j = \{x, y, z\}$.

DFT Calculations. The DFT calculations employed the WIEN2k package,[19] which is a full potential, all electron method that utilizes the L/APW+lo approach.[30] The exchange and correlation potentials within DFT were calculated using the generalized gradient approximation.[31] In the calculations the following atomic-sphere radii (R_{MT}), given in atomic units (au), were used: H(0.45−0.6), Li(1.8), B(1.2/1.3), N(1.2), C(1.2), O(1.3/1.4), Mg(1.7), Si(1.6/1.7), and Ca(2.0). Different R_{MT} values have been used for B, O, and Si to obtain nonoverlapping spheres for the different geometries of the BO_3/BO_4 and SiO_4 units. For the H atom the range of R_{MT} values reflects the variation in bond distances associated with the different H species. In all cases the core electron states were separated from the valence states at −6.0 Ry. However, to avoid core-charge leakage from the atomic sphere for Si, a separation energy of −7.8 Ry was used to include the 2p orbitals of Si in the valence states. Calculations were performed at a plane-wave cutoff defined by $\min(R_{MT})\max(k_n)$ of 2.5−2.6 and 5.5−5.7 for compounds with and without hydrogen atoms, respectively. This corresponds to approximately 5000 plane waves in the calculation for triclinic $Mg_2B_2O_5$ and 10000 plane waves for $CaB_3O_4(OH)_3{\cdot}H_2O$. In all calculations the total number of k-points in the Brillouin zone was varied and it was observed that relatively few k-points were needed (below 125 k-points) to achieve a good convergence, in agreement with the expectations for insulators. Thus, the irreducible Brillouin zone was sampled on shifted tetrahedral meshes varying from 6 to 32 k-points. The calculations were performed on a multinode cluster of computers and the calculation time varied from 4 to 24 h for a fixed geometry. A DFT structure optimization typically required 6−8 steps.

3. Results and Discussion

To investigate the correlation between experimental ^{11}B EFG tensor elements and those obtained from DFT calculations, lithium tetraborate ($Li_2B_4O_7$), magnesium orthoborate ($Mg_3B_2O_6$), and magnesium pyroborate ($Mg_2B_2O_5$) are studied by ^{11}B MAS NMR (Figures 1 and 2). Furthermore, we have also included the ^{11}B quadrupole coupling parameters for the tetrahedrally coordinated boron site in $NH_4B(C_6H_5)_4$ (tetragonal, space group $I\bar{4}2m$)[32] and for the BO_3 and the two BO_4 sites in colemanite ($CaB_3O_4(OH)_3{\cdot}H_2O$, monoclinic, space group $P2_1/a$),[33] recently

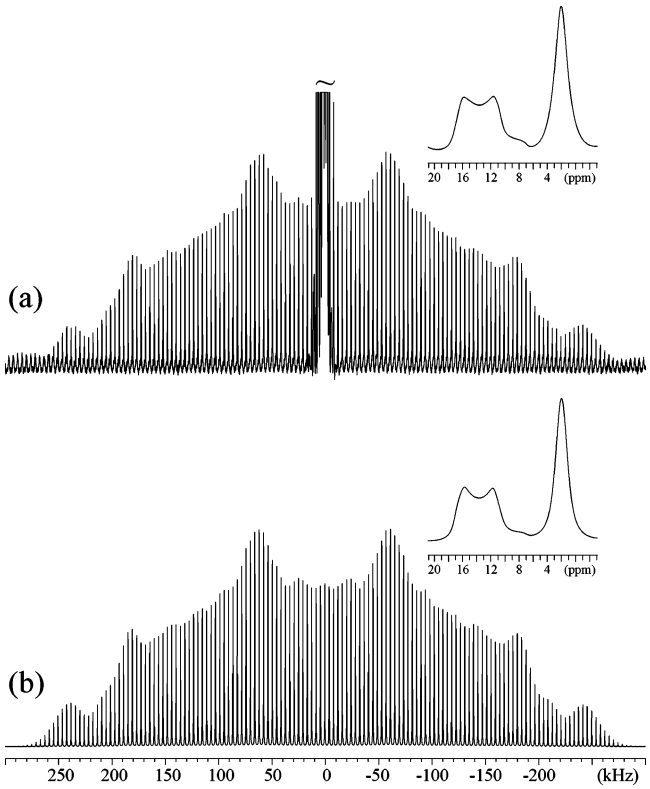

Figure 1. (a) ^{11}B MAS NMR spectrum of $Li_2B_4O_7$, recorded at 14.1 T using a spinning speed $\nu_R = 4100$ Hz. The spectrum illustrates the manifold of ssbs from the satellite transitions for the BO_4 site whereas the inset shows the centerbands from the central transition for the BO_3 and BO_4 sites. The ssbs in the outer regions of the spectrum originate from the satellite transitions for the BO_3 site. (b) Simulated spectrum resulting from optimization to the manifold of ssbs from the satellite transitions for the BO_4 site only. The inset illustrates the optimized simulation of the centerbands for the BO_3 and BO_4 sites. The C_Q, η_Q, and δ_{iso} parameters for the two sites in $Li_2B_4O_7$ are listed in Table 1.

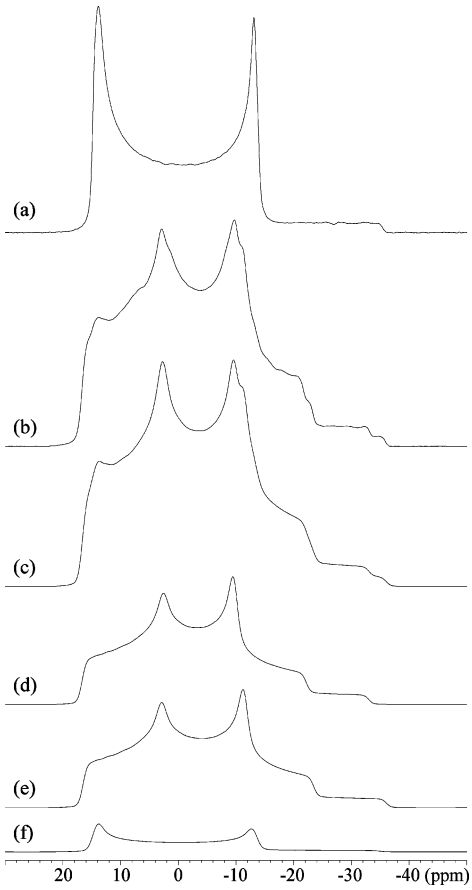

Figure 2. ^{11}B MAS NMR spectra (7.1 T, $\nu_R = 10.0$ kHz) of the central transition for (a) $Mg_3B_2O_6$ and (b) $Mg_2B_2O_5$. (c) Optimized simulation of the centerband in (b) employing the sum of the quadrupolar line shapes shown in (d)−(f) for the two BO_3 sites in $Mg_2B_2O_5$ and the BO_3 site for an impurity of $Mg_3B_2O_6$ in the sample. The C_Q, η_Q, and δ_{iso} parameters are listed in Table 1. (d) and (e) correspond to the BO_3 sites Δ_1 and Δ_2, respectively.

reported from ^{11}B MAS and single-crystal NMR (14.1 T), respectively.[17] Thus, five different borate structures, which include four tetrahedrally coordinated boron sites and five BO_3 sites, are considered as model compounds for the DFT calculations. These borates all exhibit well-defined crystal structures and a variation in ^{11}B quadrupole coupling constants within the earlier reported ranges $2.4 \lesssim C_Q \lesssim 3.0$ MHz and $C_Q < 1$ MHz for BO_3 and BO_4 units, respectively.[10−17] Moreover, the crystal structures reveal that the boron atoms in the model compounds (with the exception of $NH_4B(C_6H_5)_4$) are not located at high-symmetry positions, which would result in constraints on the EFG tensor orientations in the crystal frames. The ^{11}B quadrupole coupling parameters (C_Q and η_Q), isotropic chemical shifts (δ_{iso}), and the calculated EFG tensor elements (V_{xx}, V_{yy}, V_{zz}) are listed in Table 1 for the studied model compounds. It is noted that ^{11}B chemical shift anisotropies (CSAs, $\delta_\sigma = \delta_{iso} - \delta_{zz}$) of magnitude $|\delta_\sigma|$ from 10 to 22 ppm and $|\delta_\sigma| \lesssim 10$ ppm have been reported for inorganic borates containing BO_3 sites[16] and BO_4 units,[17] respectively. Such small CSAs imply that the effect of this interaction can be neglected when the ^{11}B MAS NMR spectra are recorded with a high spinning speed, even at a magnetic field of 14.1 T. Thus, the analysis of the ^{11}B MAS NMR spectra in this work does not consider the ^{11}B CSA whereas this interaction was included in the simulations of the ^{11}B MAS and single-crystal NMR spectra for $NH_4B(C_6H_5)_4$ and colemanite.[17]

^{11}B MAS NMR of Model Compounds. Figure 1a illustrates the ^{11}B MAS NMR spectrum of the central and satellite transitions for $Li_2B_4O_7$. The tetraborate unit in $Li_2B_4O_7$ contains two crystallographically equivalent BO_4 and BO_3 units.[34] This is in agreement with the ^{11}B MAS NMR spectrum (14.1 T), which shows resonances from such two sites exhibiting a small and a large quadrupole coupling, respectively. The ^{11}B quadrupole coupling parameters for the BO_3 site are accurately determined from least-squares optimization to the centerband and first- and second-order spinning sidebands (ssbs) from the central transition, giving the C_Q, η_Q, and δ_{iso} parameters listed in Table 1. The determination of the corresponding parameters for the BO_4 site utilizes the manifold of ssbs, observed over a spectral range of approximately 500 kHz, in a least-squares analysis to the experimental ssb intensities. This procedure along with an error-analysis[29] results in C_Q and η_Q parameters of high precision (Table 1) and the simulated spectrum of the satellite transitions shown in Figure 1b.

Figure 2a and b illustrate the central transition observed in the ^{11}B MAS NMR spectra (7.1 T) of $Mg_3B_2O_6$ and $Mg_2B_2O_5$, respectively. The second-order quadrupolar line shape for $Mg_3B_2O_6$ can be simulated to high precision using a single set of C_Q, η_Q, and δ_{iso} parameters (Table 1), in agreement with the orthorhombic crystal structure reported for magnesium orthoborate.[35] The ^{11}B NMR parameters, obtained from this simulation for $Mg_3B_2O_6$, are in excellent agreement with the parameters reported by Kroeker and Stebbins[16] from a ^{11}B MAS NMR spectrum of $Mg_2B_2O_5$, which contained an impurity of $Mg_3B_2O_6$. The splitting of the low-frequency singularity (−10 ppm) and

TABLE 1: Experimental ^{11}B NMR Parameters (C_Q, η_Q, δ_{iso}) and EFG Tensor Elements (V_{xx}, V_{yy}, V_{zz}) from DFT Calculations for the Borates Studied in This Work

compound	site[a]	δ_{iso} (ppm)	$\lvert C_Q^{exp}\rvert$ (MHz)	η_Q^{exp}	C_Q^{calc} (MHz)	η_Q^{calc}	V_{xx} (10^{21}V /m^2)	V_{yy} (10^{21}V /m^2)	V_{zz} (10^{21}V /m^2)	ref[b]
$Li_2B_4O_7$	T	2.2 ± 0.1	0.52 ± 0.02	0.51 ± 0.02	−0.54	0.52	0.42	0.13	−0.55	34
	Δ	18.1 ± 0.2	2.56 ± 0.03	0.21 ± 0.04	2.54	0.19	−1.52	−1.04	2.56	
$NH_4B(C_6H_5)_4$[c]	T	−7.9 ± 0.3	0.029 ± 0.001	0.00	0.04	0	−0.02	−0.02	0.04	32
$Mg_2B_2O_5$	Δ_1	18.6 ± 0.1	2.71 ± 0.02	0.50 ± 0.02	2.72	0.50	−2.05	−0.69	2.74	25
(triclinic)	Δ_2	19.0 ± 0.1	2.81 ± 0.02	0.45 ± 0.02	2.83	0.46	−2.08	−0.77	2.85	
$Mg_3B_2O_6$	Δ	22.6 ± 0.1	2.93 ± 0.01	0.03 ± 0.02	2.97	0.02	−1.53	−1.47	3.00	35
$CaB_3O_4(OH)_3{\cdot}H_2O$[c]	Δ	17.1 ± 0.3	2.543 ± 0.005	0.055 ± 0.004	2.49	0.04	−1.30	−1.21	2.51	33
(colemanite)	T_1	1.2 ± 0.2	0.440 ± 0.001	0.499 ± 0.003	−0.49	0.38	0.34	0.15	−0.49	
	T_2	1.2 ± 0.2	0.312 ± 0.001	0.809 ± 0.003	−0.32	0.54	0.25	0.08	−0.33	
$CaBSiO_4(OH)$[c]	T	0.2 ± 0.2	0.172 ± 0.001	0.647 ± 0.005	0.28	0.79	−0.25	−0.03	0.28	43
(datolite)					0.16	0.50	−0.12	−0.05	0.17	Opt
$CaB_2Si_2O_8$	T	−0.2 ± 0.1	0.39 ± 0.02	0.43 ± 0.03	−0.44	0.52	0.34	0.10	−0.44	44
(danburite)					−0.40	0.37	0.27	0.13	−0.40	Opt

[a] Parameters for tetrahedral (T) and trigonal (Δ) coordinated boron. [b] References for the crystal structures used in the DFT calculations. Opt denotes refined structures (this work). [c] The experimental ^{11}B NMR data are taken from ref 17. The parameters for colemanite and datolite are obtained by ^{11}B single-crystal NMR whereas ^{11}B MAS NMR was employed for $NH_4B(C_6H_5)_4$.

the two edges at low frequency (−32 and −35 ppm) of the centerband observed for $Mg_2B_2O_5$ (Figure 2b) indicate the presence of two overlapping quadrupolar line shapes with similar intensities and quadrupole couplings. Furthermore, by comparison of the spectrum in Figure 2b with Figure 2a, it is apparent that the low-intensity, high-frequency singularity at 14 ppm originates from a minor impurity of $Mg_3B_2O_6$. Thus, the optimized fitting of the spectrum in Figure 2b employs two quadrupolar line shapes with equal intensity and a third resonance corresponding to the C_Q, η_Q, and δ_{iso} parameters determined for magnesium orthoborate. This gives the parameters for $Mg_2B_2O_5$ listed in Table 1 and the optimized simulation in Figure 2c, which corresponds to the addition of the individual line shapes shown in Figure 2d−f. The C_Q, η_Q, and δ_{iso} parameters for the two sites in $Mg_2B_2O_5$ are confirmed by simulations of a similar ^{11}B MAS spectrum recorded at 14.1 T (not shown); however, the small differences in C_Q and η_Q for the two sites are best appreciated in the spectrum at lower magnetic field (Figure 2b). The observation of two BO_3 sites in a 1:1 ratio is in accord with the crystal structure for triclinic $Mg_2B_2O_5$.[25] Moreover, the ^{11}B NMR parameters (Table 1) are very similar to the values $C_Q = 2.78 \pm 0.02$ MHz, $\eta_Q = 0.48 \pm 0.02$, and $\delta_{iso} = 18.7 \pm 0.1$ ppm reported by Kroeker and Stebbins[16] from a ^{11}B MAS spectrum (14.1 T) assuming a single ^{11}B site in $Mg_2B_2O_5$.

DFT Calculations for the Model Compounds. The DFT calculations are performed using the L/APW+lo approach[30] and the generalized gradient approximation by Perdew, Burke, and Enzerhof[31] (PBE-GGA) for calculation of the exchange and correlation potentials. The PBE-GGA represents the most systematically constructed GGA and from the comparative study of different functionals by Kurth et al.,[36] the PBE-GGA is expected to give the best results, especially for structure optimizations. Both the local density approximation (LDA)[37] and GGA are expected to give reliable results for the charge densities in calculations where the atomic coordinates are fixed. However, in a study of fosterite (Mg_2SiO_4), improved values for the calculated EFGs were obtained using the GGA method as compared to the LDA.[38]

The DFT calculations in this work employ the atomic coordinates and unit cell parameters reported for the model borate compounds from single-crystal X-ray or neutron diffraction.[25,32−35] The calculated EFG tensor elements (V_{xx}, V_{yy}, V_{zz}), listed in Table 1 for the model compounds, are compared with the principal elements of the experimental quadrupole coupling tensors ($Q_{ii}^{exp} = (eQ/h)V_{ii}^{exp}$, $i = x, y, z$) defined as

$$Q_{zz}^{exp} = C_Q$$

$$Q_{yy}^{exp} = -\frac{1}{2}(1 - \eta_Q)C_Q$$

$$Q_{xx}^{exp} = -\frac{1}{2}(1 + \eta_Q)C_Q \qquad (2)$$

The sign of the quadrupole coupling constant cannot be determined from single-pulse NMR experiments and thus, the C_Q values listed in Table 1 correspond to $|C_Q|$. However, the DFT calculations provide the absolute sign of the EFG tensor elements, and thus, it is assumed that the experimental C_Q values exhibit the same sign as the corresponding calculated V_{zz}^{calc} elements. This approach is employed in Figure 3, which illustrates a plot of Q_{ii}^{exp} as a function of V_{ii}^{calc} for the five model borates. The plot demonstrates a convincing linear relationship between the experimental and calculated tensor elements for the tetrahedrally coordinated boron sites as well as the BO_3 units.

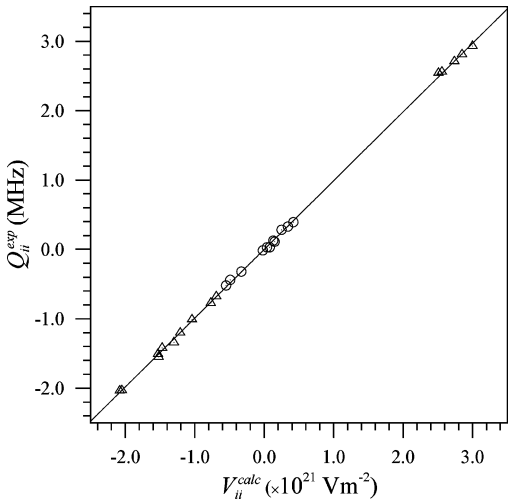

Figure 3. Linear correlation between the principal ^{11}B quadrupole coupling tensor elements (Q_{ii}^{exp}) and the corresponding calculated EFG tensor elements (V_{ii}^{calc}) from DFT calculations (WIEN2k) for the five model borates. The calculated EFG tensor elements are summarized in Table 1 and the result from linear regression analysis of the data is given in eq 3. The open circles and triangles correspond to data for the BO_4 and BO_3 sites, respectively.

Linear regression analysis of the data shown in Figure 3 gives the equation

$$Q_{ii}^{\mathrm{exp}}\,(\mathrm{MHz}) = 0.990(4)\left(\frac{\mathrm{MHz}}{10^{21}\ \mathrm{V\ m^{-2}}}\right)V_{ii}^{\mathrm{calc}}(10^{21}\ \mathrm{V\ m^{-2}}) - 0.0003(60)\ (\mathrm{MHz}) \quad (3)$$

with the correlation coefficient $R = 0.9998$. From this linear relationship the calculated ^{11}B quadrupole coupling parameters ($C_{\mathrm{Q}}^{\mathrm{calc}}$ and $\eta_{\mathrm{Q}}^{\mathrm{calc}}$) are obtained and listed in Table 1. The parameters in Table 1 reveal that the differences between the experimental and calculated C_{Q}, η_{Q} values are within the error limits for the experimental data determined from ^{11}B MAS NMR, except for the C_{Q} value of the BO_3 site in $Mg_3B_2O_6$ (i.e., $C_{\mathrm{Q}}^{\mathrm{exp}} - C_{\mathrm{Q}}^{\mathrm{calc}} = 0.04$ MHz). Minor deviations are also observed for the data reported from ^{11}B single-crystal NMR, where the error limits are significantly smaller. We also note that the DFT calculations excellently reproduce the small difference in quadrupole coupling parameters for the two BO_3 sites in $Mg_2B_2O_5$ using the crystal-structure data.[25]

Although, a convincing agreement between the experimental and calculated C_{Q}, η_{Q} values is achieved for the model compounds, it is of interest to study the possibility of improving the calculated EFG elements by DFT structural refinements of the crystal structures. This is investigated for $Li_2B_4O_7$ using the XRD fractional atomic coordinates for this borate as starting values for a DFT optimization of the atomic coordinates by minimization of the forces between the nuclei.[30] The optimized fractional atomic coordinates are given as Supporting Information and results in the calculated parameters $C_{\mathrm{Q}}^{\mathrm{ref}} = 2.53$ MHz, $\eta_{\mathrm{Q}}^{\mathrm{ref}} = 0.19$ and $C_{\mathrm{Q}}^{\mathrm{ref}} = -0.58$ MHz, $\eta_{\mathrm{Q}}^{\mathrm{ref}} = 0.56$ for the BO_3 and BO_4 units, respectively. These values are almost identical to those calculated from fixed atomic coordinates from XRD (Table 1) and within the uncertainty limits of the experimental values for the BO_3 site. However, for the BO_4 tetrahedron the calculated parameters using fixed atomic coordinates (from XRD) agree slightly better with the experimental data (i.e., $C_{\mathrm{Q}}^{\mathrm{exp}} - C_{\mathrm{Q}}^{\mathrm{calc}} = 0.02$ MHz, $\eta_{\mathrm{Q}}^{\mathrm{exp}} - \eta_{\mathrm{Q}}^{\mathrm{calc}} = -0.01$) as compared to the values obtained after DFT optimization (i.e., $C_{\mathrm{Q}}^{\mathrm{exp}} - C_{\mathrm{Q}}^{\mathrm{ref}} = 0.04$ MHz, $\eta_{\mathrm{Q}}^{\mathrm{exp}} - \eta_{\mathrm{Q}}^{\mathrm{ref}} = -0.05$). Furthermore, a comparison of the B−O bond lengths before and after DFT optimization shows that the B−O bond lengths from the optimized structure are slightly longer than those reported from X-ray diffraction for all bonds. For the BO_3 unit the difference is in the range 0.009−0.013 Å whereas differences of 0.005−0.018 Å are found for the BO_4 tetrahedron. Overall, the DFT optimization for $Li_2B_4O_7$ and the calculated and experimental C_{Q}, η_{Q} parameters suggest that an improvement of the atomic coordinates for this borate is not achieved from the DFT structure optimization. Moreover, we expect that a similar result may be achieved for the other model compounds studied in this work, considering the excellent agreement between the experimental and calculated C_{Q}, η_{Q} values (Table 1) and the fact that crystal structures have been reported within the last two decades for these borates.

^{11}B Nuclear Quadrupole Moment. The linear relationship between Q_{ii}^{exp} and V_{ii}^{calc}, observed for the model borate compounds (eq 3), allows calculation of the ^{11}B nuclear quadrupole moment (Q) from the slope ($a = eQ/h$) in Figure 3. This gives the quadrupole moment $Q = 0.0409 \pm 0.0002$ barn (b = barn, 1 b = 10^{-28} m^2), which is in excellent agreement with the value $Q = 0.0406 \pm 0.0001$ b reported for ^{11}B in recent compilations of nuclear quadrupole moments.[39,40] This recommended quadrupole moment was determined from multiconfigurational Hartree−Fock calculations of the electric field gradients for the bare boron atom, derived from the hyperfine structure of B(^{2}P), combined with the experimental nuclear quadrupole coupling constant obtained from atomic-beam magnetic resonance measurements.[41,42] The excellent agreement between the $Q(^{11}\mathrm{B})$ value reported from that study and the value derived from Figure 3 strongly supports that the WIEN2k DFT calculations can provide highly accurate ^{11}B quadrupole coupling parameters on an absolute scale. We note that DFT calculations have earlier been used in a redetermination of the nuclear quadrupole moment for ^{57}Fe from the slope of the linear correlation between theoretical EFGs and experimental quadrupole splittings determined from Mössbauer spectroscopy.[22]

Orientation of the ^{11}B EFG Tensors. Another important feature of the calculations is the ability to provide the full orientation of the EFG tensor in the crystal frame, a kind of information that can only be obtained experimentally from single-crystal NMR. Thus, the WIEN2k calculations may be useful in structural interpretations of quadrupole coupling parameters derived from NMR studies of polycrystalline powders. We note that the symmetry of the EFG tensor implies that the direction of V_{xx} and V_{yy} cannot be distinguished from the $-V_{xx}$ and -V_{yy} directions, respectively. The orientation of the EFG tensor elements for the ^{11}B sites in the tetraborate unit of $Li_2B_4O_7$ and in the pyroborate unit of $Mg_2B_2O_5$ are illustrated in Figure 4a,b, respectively (the direction cosines, describing the orientation for the elements within the crystal frames, are given in the Supporting Information). The BO_3 sites in both of these units exhibit EFG tensors with the unique elements (V_{zz}) aligned almost perpendicular to the trigonal plane. Obviously, this orientation of V_{zz} is imposed by the nearly trigonal symmetry of the BO_3 units. Thus, the V_{zz} elements are oriented along the p_z orbital of boron, which exhibits a deficiency in negative charge as compared to the σ-bonding p_x and p_y orbitals. The orientation of V_{zz} perpendicular to the trigonal plane is a general feature for BO_3 units, which explains the positive sign of the V_{zz} elements calculated for the BO_3 units in this work (Table 1). The orientation of V_{xx} and V_{yy} for the BO_3 units in Figure 4 indicates that the numerically smallest EFG tensor element (V_{yy}) is oriented nearly along the longest B−O bond. This is in accordance with our expectations and with the electron density map for the $B_2O_5^{4-}$ unit of $Mg_2B_2O_5$ shown in Figure 5, because the smallest electron density in the BO_3 plane is found along the longest B−O bond. Moreover, for the BO_3 units in $Mg_2B_2O_5$ (Figure 4b), the B−O−B bonds are significantly longer than the nonbridging B−O bonds. This fact may explain the larger values of η_{Q} for the BO_3 units in $Mg_2B_2O_5$ as compared to η_{Q} for BO_3 in $Li_2B_4O_7$ (cf., Table 1). An interpretation of the EFG tensor orientation for the BO_4 site in $Li_2B_4O_7$ (Figure 4a) is less straightforward, because the three elements are situated between the B−O bonds of the distorted BO_4 tetrahedron. However, the V_{zz} element is oriented in the same direction as the shortest B−O bond, corresponding to the direction of highest electron density. This is opposite the orientation of the V_{zz} element for the BO_3 sites and accounts for the negative sign of V_{zz} for the BO_4 site in $Li_2B_4O_7$. Similar orientations (not shown) and negative values of V_{zz} are also observed for the two BO_4 tetrahedra in colemanite (Table 1).

Optimization of the Crystal Structures for Datolite and Danburite. The correlation between experimental and calculated ^{11}B quadrupole coupling parameters has also been investigated for the borate minerals datolite ($CaBSiO_4(OH)$) and danburite ($Ca_2BSi_2O_8$), which both include a single BO_4 tetrahedron in the asymmetric unit.[43,44] The ^{11}B NMR parameters are deter-

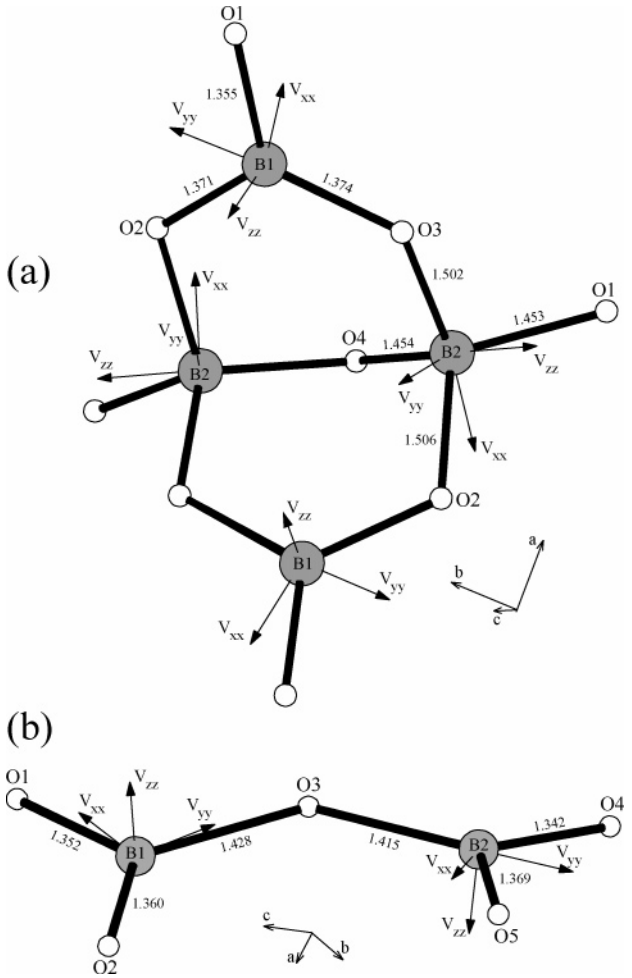

Figure 4. Projections of the calculated EFG tensors for the boron sites in (a) the tetraborate unit of $Li_2B_4O_7$ and (b) the pyroborate unit of $Mg_2B_2O_5$. The boron and oxygen atoms are labeled according to the reported crystal structures[25,34] used as input for the DFT calculations. It is noted that the direction of V_{xx} and V_{yy} cannot be distinguished from the $-V_{xx}$ and $-V_{yy}$ directions, respectively.

mined with good precision (Table 1) for danburite from least-squares optimization to the manifold of ssbs observed for the satellite transitions (Figure 6) whereas the parameters reported in a recent ^{11}B single-crystal NMR study of datolite[17] is adopted here. Employing the crystal structure data reported from single-crystal XRD for datolite[43] and danburite[44] as input to the DFT calculations results in the calculated parameters $C_Q^{calc} = 0.28$ MHz, $\eta_Q^{calc} = 0.79$ and $C_Q^{calc} = -0.44$ MHz, $\eta_Q^{calc} = 0.52$ for datolite and danburite, respectively. Comparison of these parameters with the experimental data (Table 1) demonstrates larger deviations than observed for the model compounds. These deviations may possibly reflect the fact that the crystal structures were reported more than three decades ago and, thereby, that the XRD data are of lower precision as compared to the more recent crystal structures reported for the model compounds. Although, improved structural data may be obtained using todays X-ray diffraction technology, the possibility of refining the structures using DFT calculations is investigated for datolite and danburite. The quality of the optimized structures is validated by comparing the calculated EFGs with the experimental data.

The optimization employs the XRD fractional atomic coordinates as starting values. After a definition of the step lengths, the atomic coordinates are optimized by minimization of the forces between the nuclei.[30] This method is first applied to the crystal structure of datolite, which contains sheets of alternating SiO_4 and BO_3OH tetrahedra.[43] The resulting B−O and O−H bond lengths are listed in Table 2 whereas the optimized set of atomic coordinates is given as Supporting Information. The largest differences between the bond lengths before and after optimization are observed for B−O4 (0.017 Å) and O5−H (0.014 Å), whereas the differences between the remaining bonds are below 0.01 Å. In an XRD structure determination, it may be hard to accurately obtain the O−H bond length due to the nonspherical nature of the electron density for the hydrogen atom.[45] This problem is reflected in the experimental O−H bond length of 0.75(5) Å (Table 2) determined by XRD, which is significantly shorter than the (B−)O−H bond lengths reported from neutron diffraction studies of inorganic borates. Two examples are the O−H distances 0.958 and 0.982 Å, in the tetraborate unit ($B_4O_5(OH)_4^{2-}$) of Borax ($Na_2B_4O_5(OH)_4 \cdot 8H_2O$),[46] and the O−H distances 0.995 and 1.031 Å for bakerite ($Ca_4B_5Si_3O_{15}(OH)_5$), which is structurally related to datolite.[47] The optimized value for the O−H distance in datolite (Table 2) is in excellent agreement with the B−O distance reported for the very similar BO_3OH tetrahedra in bakerite. Furthermore, it is gratifying that the optimization also strongly improves the agreement between C_Q^{calc} and C_Q^{exp} (Table 1). This emphasizes the reliability of the optimized structure but also shows that the EFGs can be used as a structural fingerprint. The improved agreement between C_Q^{exp} and C_Q^{calc} as compared to that for the corresponding asymmetry parameters, reflects the fact that η_Q^{calc} is the scaled difference between V_{xx} and V_{yy} and that these elements are of similar magnitude.

The DFT approach for optimization of crystal structures is also investigated for danburite (the optimized set of atomic coordinates is given as Supporting Information). The B−O bond lengths for the BO_4 tetrahedron in danburite before and after the DFT optimization are listed in Table 2 and a comparison of these values shows deviations less than 0.01 Å. Danburite contains no H atoms, and the reported structure is therefore less controversial than the XRD structure of datolite. However, it is apparent that the ^{11}B parameters calculated from the optimized structure (Table 1) demonstrate an improvement when compared to the experimental values. The largest change in fractional atomic coordinates is observed for the O4 atom (XRD: $x = 0.5136$, $y = 0.6636$, $z = 0.2500$, DFT: $x = 0.5198$, $y = 0.6607$, $z = 0.2500$). Although, the O4 atom is not directly bonded to boron, this difference may also affect the ^{11}B EFG tensor derived from the DFT calculation. This reflects the high sensitivity of the calculated EFG tensors to even small variations in the local geometry of the nearest coordination sphere.

The improved agreement between experimental and calculated EFGs for datolite and danburite is best appreciated by the plot in Figure 7, which illustrates the experimental quadrupole tensor elements as a function of the calculated EFG tensor elements before and after DFT optimization. The improved correlation after the DFT optimization is in full accord with the results obtained for the model compounds, which are illustrated in Figure 7 by the line corresponding to a plot of eq 3. These observations strongly suggests that improvements of the fractional atomic coordinates for datolite and danburite are achieved by the DFT optimizations as compared to the earlier reported XRD structural data.[43,44]

Finally, Figure 8 illustrates the orientation of the calculated ^{11}B EFG tensors for the BO_4 tetrahedra in danburite and datolite. For danburite the unique element (V_{zz}) is oriented along the shortest B−O bond (i.e., the B−O−B bond of the $B_2O_7^{8-}$ unit) whereas the numerically smallest element (V_{yy}) is close to the

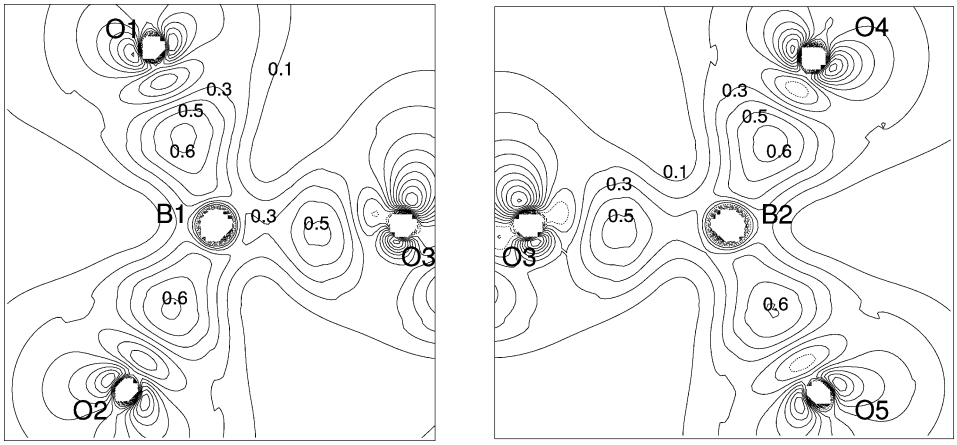

Figure 5. Contour plots of the deformation densities for the two borate units of $Mg_2B_2O_5$ (Figure 4b): (a) BO_3 plane defined by B1, O3, and O1; (b) BO_3 plane defined by B2, O3, and O4. Contours are plotted at 0.1 e/Å^3. Broken lines and the dotted line, which represent negative contours and the zero contour, respectively, are found solely close to the core regions.

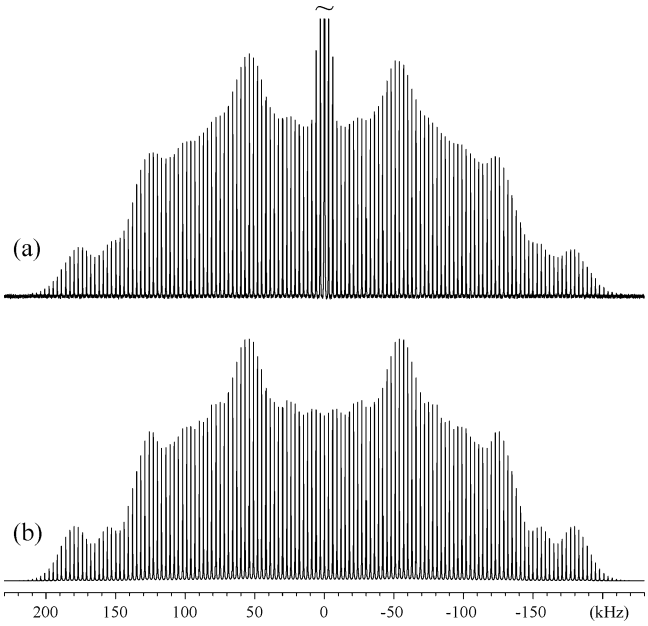

Figure 6. (a) ^{11}B MAS NMR spectrum (14.1 T, $\nu_R = 3.0$ kHz) of the satellite transitions for danburite ($CaB_2Si_2O_8$). The centerband from the central transition is cutoff at about $^1/_{50}$th of its total height. (b) Optimized simulation of the manifold of ssbs from the satellite transitions, corresponding to the C_Q, η_Q, and δ_{iso} parameters listed in Table 1.

direction of the longest B−O bond. Thus, the orientation of V_{zz} in the BO_4 tetrahedron is in the direction of highest electron density, which accounts for the negative sign of V_{zz}, in agreement with the observation for the EFG tensor of the BO_4 site in $Li_2B_4O_7$ (Figure 4a). On the contrary, the V_{zz} element for the BO_3OH tetrahedron in datolite is situated along the longest B−O bond (i.e., the B−O−H bond), corresponding to the direction of lowest electron density in the BO_4 tetrahedron. This is in accordance with the positive sign of V_{zz}, in full analogy to the EFG orientations observed for the BO_3 sites studied in this work (Figure 4, vide supra).

4. Conclusions

The present study demonstrates the strong potential of combining DFT (WIEN2k) calculations with experimental ^{11}B NMR data in the characterization and refinement of borate structures. This potential is emphasized by the convincing correlation observed between the experimental quadrupole coupling tensor elements and the corresponding calculated EFG values for BO_4 and BO_3 units in a number of model borate compounds. The ^{11}B quadrupole moment (Q), derived from this

TABLE 2: Bond Lengths for the BO_4 Tetrahedra in Datolite ($CaBSiO_4(OH)$) and Danburite ($CaB_2Si_2O_8$) from XRD and the DFT Optimized Structures

	bond	XRD[a] (Å)	DFT[b] (Å)
$CaBSiO_4(OH)$	B−O2	1.475(3)	1.488
(datolite)	B−O3	1.486(3)	1.484
	B−O4	1.463(3)	1.480
	B−O5	1.496(3)	1.503
	O5−H	0.75(5)	0.99
$CaB_2Si_2O_8$	B−O1	1.479(2)	1.486
(danburite)	B−O2	1.498(2)	1.503
	B−O3	1.461(2)	1.467
	B−O5	1.456(2)	1.461

[a] Bond lengths from the reported crystal structures (single-crystal X-ray diffraction) for datolite[43] and danburite.[44] [b] Calculated bond lengths from the refined structures by DFT optimization of all atomic positions.

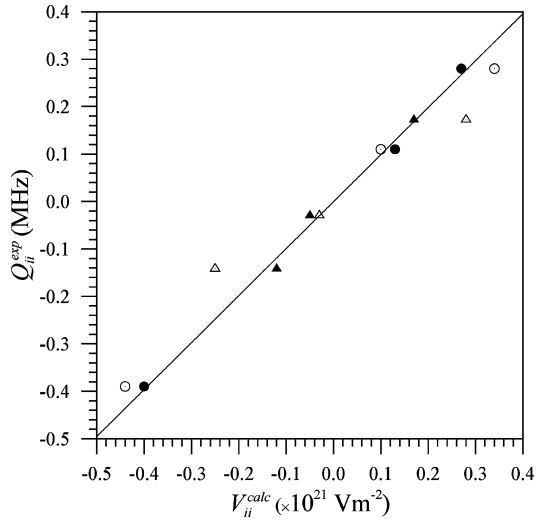

Figure 7. Correlation between the principal ^{11}B quadrupole coupling tensor elements (Q_{ii}^{exp}) and the corresponding calculated EFG tensor elements (V_{ii}^{calc}) from DFT calculations for the BO_4 tetrahedra in danburite (circles) and datolite (triangles). The open symbols correspond to the DFT calculations using the reported XRD structures[43,44] whereas filled symbols illustrate the results obtained after the DFT structural refinements. The calculated EFG tensor elements are summarized in Table 1. The straight line corresponds to the linear correlation obtained for the model compounds (eq 3).

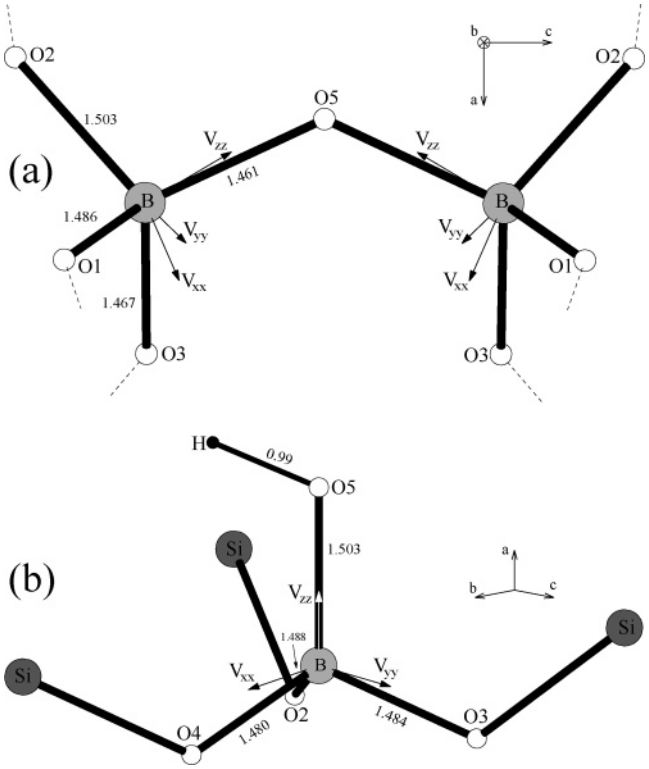

Figure 8. Projections of the calculated EFG tensors for the tetahedral boron sites in (a) danburite and (b) datolite. The boron and oxygen atoms are labeled according to the reported crystal structures.[43,44] The oxygen atoms O1, O2, and O3 of the $B_2O_7^{8-}$ unit in danburite are bonded to Si (dashed lines) in the framework structure. In the projection of the BO_3OH unit for datolite, the V_{zz} element (white arrow) is situated slightly in front of the B−O5 bond. The black shaded circles represent Si atoms bonded to the O2, O3, and O4 oxygen atoms of the BO_3OH unit.

correlation, is in full accord with the value reported from ab initio calculations combined with atomic-beam magnetic resonance measurements for the bare boron atom. This fact strongly indicates that reliable ^{11}B quadrupole coupling tensors can be obtained from WIEN2k calculations. These results have been utilized in a refinement of the crystal structures for the borate minerals danburite ($Ca_2BSi_2O_8$) and datolite ($CaBSiO_4(OH)$) using the experimental ^{11}B quadrupole coupling data as quality parameters for the refinements. The DFT calculations for danburite have demonstrated that the ^{11}B EFG tensors are highly sensitive to small variations in the atomic coordinates, reflected by deviations for the B−O bond lengths of less than 0.01 Å for the structures before and after optimization. The refinement of the structure for datolite mainly concerns the unusually short O−H bond length, previously reported from XRD.[43] However, the DFT calculations provide a more reliable value that is very similar to the O−H bond lengths reported for other inorganic borates from neutron diffraction. Thus, DFT structural refinements may be particularly useful for inorganic structures containing O−H bonds, because the exact positions of these hydrogens are difficult to obtain from standard XRD studies. Finally, the DFT calculations have provided useful structural information by determination of the sign for the ^{11}B quadrupole coupling constants and the orientation of the EFG tensors in the crystal frame. For the BO_4 and BO_3 units investigated in this work, it has been observed that a positive sign for the unique EFG tensor element (V_{zz} and thereby C_Q) reflects this element to be oriented in the direction of lowest electron density. For the BO_3 units this correspond to V_{zz} being oriented perpendicular to the BO_3 plane. On the other hand, a negative sign for V_{zz} shows that this element is located in the direction of highest electron density, for example along the shortest B−O bond as observed for the BO_4 tetrahedra in $Li_2B_4O_7$ and danburite.

Acknowledgment. The use of the facilities at the Instrument Centre for Solid-State NMR Spectroscopy, University of Aarhus, sponsored by the Danish Natural Science Research Council, the Danish Technical Science Research Council, Teknologistyrelsen, Carlsbergfondet, and Direktør Ib Henriksens Fond, is acknowledged. We thank the Danish Technical Science Research Council (J. No. 26-03-0049, M.R.H.) and the Carlsberg foundation (G.K.H.M.) for financial support. We acknowledge support from the Danish Center for Scientific Computing (DCSC). Ole Johnsen, the Geological Museum, University of Copenhagen is acknowledged for providing the mineral sample of danburite.

Supporting Information Available: Direction cosines describing the orientation of the calculated EFG tensors elements for ^{11}B in the crystal structures of $Li_2B_4O_7$, $Mg_2B_2O_5$, danburite ($CaB_2Si_2O_8$), and datolite ($CaBSiO_4(OH)$). Optimized fractional atomic coordinates for $Li_2B_4O_7$, danburite, and datolite from DFT calculations. This material is available free of charge via the Internet http://pubs.acs.org.

References and Notes

(1) Keszler, D. A. In *Encyclopedia of Inorganic Chemistry*; King, R. B. Ed.; J. Wiley & Sons: Chichester, U.K., 1997; Vol. 1, p 318.
(2) Millini, R.; Perego, G.; Bellussi, G. *Top. Catal.* **1999**, *9*, 13.
(3) Xiao, F. S.; Qiu, S.; Pang, W.; Xu, R. *Adv. Mater.* **1999**, *11*, 1091.
(4) Khimyak, Y. Z.; Klinowski, J. *J. Mater. Chem.* **2002**, *12*, 1079.
(5) Bautista, F. M.; Campelo, J. M.; Garcia, A.; Luna, D.; Marinas, J. M.; Moreno, M. C.; Romero, A. A.; Navio, J. A.; Macias, M. *J. Catal.* **1998**, *173*, 333.
(6) Sato, S.; Kuroki, M.; Sodesawa, T.; Nozaki, F.; Maciel, G. E. *J. Mol. Catal. A* **1995**, *104*, 171.
(7) Flego, C.; Parker Jr., W. O. *Appl. Catal A* **1999**, *185*, 137.
(8) Silver, A. H.; Bray, P. J. *J. Chem. Phys.* **1958**, *29*, 984.
(9) Bray, P. J.; Edwards, J. O.; O'Keefe, J. G.; Ross, V. F.; Tatsuzaki, I. *J. Chem. Phys.* **1961**, *35*, 435.
(10) Bray, P. J. *Inorg. Chim. Acta* **1999**, *289*, 158.
(11) Turner, G. L.; Smith, K. A.; Kirkpatrick, R. J.; Oldfield, E. *J. Magn. Reson.* **1986**, *67*, 544.
(12) Müller, D.; Grimmer, A. R.; Timper, U.; Heller, G.; Shakibai-Moghadam, M. *Z. Anorg. Allg. Chem.* **1993**, *619*, 1262.
(13) van Wüllen, L.; Müller-Warmuth, W.; Papageorgiou, D.; Pentinghaus, H. J. *J. Non-Cryst. Solids* **1994**, *171*, 53.
(14) Stebbins, J. F.; Zhao, P.; Kroeker, S. *Solid State Nucl. Magn. Reson.* **2000**, *16*, 9.
(15) Martens, R.; Müller-Warmuth, W. *J. Non-Cryst. Solids* **2000**, *265*, 167.
(16) Kroeker S.; Stebbins, J. F. *Inorg. Chem.* **2001**, *40*, 6239.
(17) Hansen, M. R.; Vosegaard, T.; Jakobsen, H. J.; Skibsted, J. *J. Phys. Chem. A* **2004**, *108*, 586.
(18) Dec, S. F.; Maciel, G. E. *J. Magn. Reson.* **1990**, *87*, 153.
(19) Blaha, P.; Schwarz, K.; Madsen, G. K. H.; Kvasnicka, D.; Luitz, J. *WIEN2k, An Augmented Plane Wave Plus Local Orbitals Program for Calculating Crystal Properties;* Vienna University of Technology: Austria, 2001; ISBN 3-9501031-1-2.
(20) Schwarz, K.; Blaha, P. *Comput. Mater. Sci.* **2003**, *28*, 259.
(21) Blaha, P.; Schwarz, K.; Dederichs, P. H. *Phys. Rev. B* **1988**, *37*, 2792.
(22) Dufek, P.; Blaha, P.; Schwarz, K. *Phys. Rev. Lett.* **1995**, *75*, 3545.
(23) Blaha, P.; Schwarz, K.; Faber, W.; Luitz, J. *Hyp. Int.* **2000**, *126*, 389.
(24) Bryant, P. L.; Harwell, C. R.; Wu, K.; Fronczek, F. R.; Hall, R. W.; Butler, L. G. *J. Phys. Chem. A* **1999**, *103*, 5246.
(25) Guo, G.-C.; Cheng, W.-D.; Chen, J.-T.; Huang, J.-S.; Zhang, Q.-E. *Acta Crystallogr. C* **1995**, *51*, 351.
(26) Dewar, M. J. S.; Jones, R. *J. Am. Chem. Soc.* **1967**, *89*, 2408.
(27) Skibsted, J.; Nielsen, N. C.; Bildsøe, H.; Jakobsen, H. J. *J. Magn. Reson.* **1991**, *95*, 88.
(28) Skibsted, J.; Nielsen, N. C.; Bildsøe, H.; Jakobsen, H. J. *Chem. Phys. Lett.* **1992**, *188*, 405.
(29) Skibsted, J.; Vosegaard, T.; Bildsøe, H.; Jakobsen, H. J. *J. Phys. Chem.* **1996**, *100*, 14872.

(30) Madsen, G. K. H.; Blaha, P.; Schwarz, K.; Sjöstedt, E.; Nordström, L. *Phys. Rev. B* **2001**, *64*, 195134.
(31) Perdew, J. P.; Burke, K.; Ernzerhof, M. *Phys. Rev. Lett.* **1996**, *77*, 3865.
(32) Steiner, T.; Mason, S. A. *Acta Crystallogr. B* **2000**, *56*, 254.
(33) Burns, P. C.; Hawthorne, F. C. *Can. Mineral.* **1993**, *31*, 297.
(34) Radaev, S. F.; Muradyan, L. A.; Malakhova, L. F.; Burak, Y. V.; Simonov, V. I. *Sov. Phys. Crystallogr.* **1989**, *34*, 842.
(35) Effenberger, H.; Pertlik, F. *Z. Kristallogr.* **1984**, *166*, 129.
(36) Kurth, Perdew, Blaha, *Int. J. Quantum Chem.* **1999**, *75*, 889.
(37) Kohn, W.; Sham, L. J. *Phys. Rev.* **1965**, *140*, A1133.
(38) Winkler, B.; Blaha, P.; Schwarz, K. *Am. Miner.* **1996**, *81*, 545.
(39) Harris, R. K.; Becker, E. D.; De Menezes, S. M. C.; Goodfellow, R.; Granger, P. *Pure Appl. Chem.* **2001**, *73*, 1795.
(40) Pyykkö, P. *Mol. Phys.* **2001**, *99*, 1617.
(41) Sundholm, D.; Olsen, J. *J. Chem. Phys.* **1991**, *94*, 5051.
(42) Pyykkö, P. *Z. Naturforsch.* **1992**, *47a*, 189.
(43) Foit, F. F.; Phillips, M. W.; Gibbs, G. V. *Am. Miner.* **1973**, *58*, 909.
(44) Phillips, M. W.; Gibbs, G. V.; Ribbe, P. H. *Am. Miner.* **1974**, *59*, 79.
(45) Coppens, P. *X-ray charge densities and chemical bonding*; Oxford University Press: Oxford, U.K., 1997.
(46) Levy, H. A.; Lisensky, G. C. *Acta Crystallogr. B* **1978**, *34*, 3502.
(47) Perchiazzi, N.; Gualtieri, A. F.; Merlino, S.; Kampf, A. R. *Am. Miner.* **2004**, *89*, 767.